Buletinul Ştiinţific al Universităţii "Politehnica" din Timişoara

Seria ELECTRONICĂ şi TELECOMUNICAŢII
TRANSACTIONS on ELECTRONICS and COMMUNICATIONS

Tom 49(63), Fascicola 1, 2004

Resonant Inverter Modeling for Induction Heating

Marin Tomşe[1], Viorel Popescu[2], Sorin Paşca[2]

Abstract – **Dynamic analysis of the phase-shift controlled series-resonant inverter for induction heating is presented using harmonic approximation modeling. First, the large-signal state-space model is derived and steady-state solution is obtaining. Finally, large signal equations are linearized about the steady-state equilibrium point to derive a linear small-signal model, which is used to study the small signal dynamic behavior of the resonant inverter. The results are verified using PSPICE.**

Keywords: editing, Symposium, author

I. INTRODUCTION

A phase-shift controlled series-resonant inverter (PSC-SRI) is used as the power supply for an induction heating system. This inverter has been suggested for induction heating applications because of its hardware simplicity. The phase-shift controlled series-resonant inverter has two control loops: the phase-shift control loop regulates the output power, and the frequency control loop ensures ZVS.

Most induction heating applications require heating the work-piece at a given temperature for a given time. During the heating process the load resistance and inductance varies especially when the work-piece reaches the Curie temperature. Therefore, since the load inductance is part of the resonant inductance, the resonant frequency of the system will vary. The frequency control strategy for the phase-shift controlled series-resonant inverter keeps track of the resonant frequency to maintain ZVS while switching as close as possible to resonance to minimize switching energy. Because of the high risk of MOSFET damage when ZVS is not achieved, it is important to know the response time and the reliability of the frequency control loop. At the same time, depending on the application, there might be a demand for accurate power control for a given temperature profile. Hence, the bandwidth, phase margin, and gain margin of the frequency and power control loop should be properly designed to guarantee a robust system. The small-signal model is a useful tool to analyze the performances of the control loops. It helps corroborate hardware loop measurements and it allows experimenting with several compensation schemes before they are implemented.

II. DERIVATION OF SMALL - SIGNAL MODEL FOR RESONANT INVERTER

Fig. 1 shows the diagram of the phase-shift controlled series-resonant inverter with the two control loops: phase-shift and frequency. The slow loop is the phase-shift control loop, which senses the output power, P_O and varies the phase-shift to maintain P_O at desired value. The fast loop is the frequency control loop, which senses the tank current and determines how far above resonance it should operate to maintain ZVS.

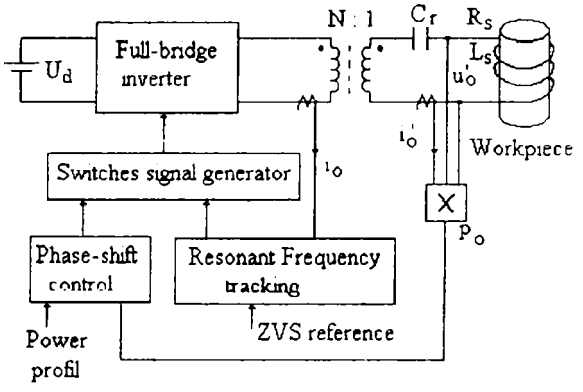

A. *Power Stage Small - Signal Model*

In this section, a summarized procedure of how to obtain the small-signal model of the power stage of the series-resonant inverter will be given.

The power stage of the circuit, a full-bridge series-resonant inverter, is shown in Fig.1. L_S and R_S are the coil plus work-piece equivalent inductance and resistance, respectively. C_r is the resonant capacitance.

[1] Facultatea de Electrotehnică şi Informatică, Str. Armatei Române, Nr. 5, Oradea, Cod 410087 , e-mail: mtomse@uoradea.ro spasca@uoradea.ro
[2] Facultatea de Electronică şi Telecomunicaţii Bd. V. Pârvan, Nr. 2, 300223 Timişoara, e-mail: vpopescu@etc.utt.ro

Also, ω_C is the switching frequency, and f_0 is the resonant frequency, where $\omega_0 = \frac{1}{\sqrt{L_s C_r}}$.

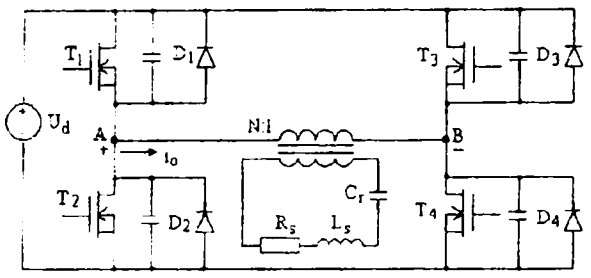

Fig.1. Series-resonant inverter power stage circuit

Power MOSFET's are selected as the switching frequency requirement. The four transistors, Q1-Q4, are operated with a 50% duty cycle.
The equivalent circuit shown in Fig.3 can represent the series-resonant inverter power stage circuit.

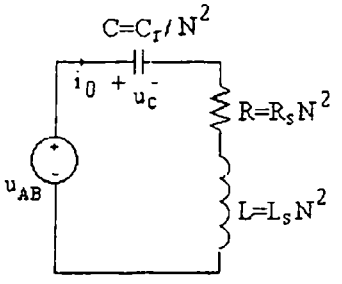

Fig.3. Equivalent series-resonant inverter circuit

First, Kirchhoff's voltage law is applied to the circuit in Fig. 3 to give:

$$C \cdot \frac{du_C}{dt} = i_0 \tag{1}$$

$$L \cdot \frac{di_0}{dt} + u_C + i_0 \cdot R = u_{AB} \tag{2}$$

The output variable is the average power at the resistance:

$$P_o = \frac{R \cdot i_0^2}{2} \tag{3}$$

The harmonic approximation is used for the inductor current, capacitor voltage and input voltage so that:

$$u_C(t) \cong u_{C_c}(t) \cdot \cos(\omega_c t) + u_{C_s}(t) \cdot \sin(\omega_c t) \tag{4}$$

$$i_0(t) \cong i_{0_c}(t) \cdot \cos(\omega_c t) + i_{0_s}(t) \cdot \sin(\omega_c t) \tag{5}$$

$$u_{AB} \cong \frac{4}{\pi} U_d \cdot \cos(\frac{\phi}{2}) \cdot \sin(\omega_c t) \tag{6}$$

Substituting (4)-(6) into (1)-(2), using the harmonic balance procedure, we can decompose (1)-(2) into four equations by grouping separately the cosine terms and the sine terms to obtain:

-cosine terms:

$$\frac{du_{C_c}}{dt} = \frac{i_{0_c}}{C} \omega_c u_{C_s} \tag{7}$$

$$\frac{di_{0_c}}{dt} = -u_{C_c} \frac{1}{L} - i_{0_c} \frac{R}{L} - \omega_c i_{0_s} \tag{8}$$

-sine terms:

$$\frac{du_{C_s}}{dt} = \frac{i_{0_s}}{C} + \omega_c u_{C_c} \tag{9}$$

$$\frac{di_{0_s}}{dt} = -u_{C_s} \frac{1}{L} - i_{0_s} \frac{R}{L} + \omega_c i_{0_c} + \frac{4}{\pi} u_d \cos(\frac{\phi}{2}) \frac{1}{L} \tag{10}$$

Equations (7)-(10) can now be used to solve for the operating point by letting all the derivatives be zero. Their solutions are:

$$U_{C_c} = \frac{\frac{4}{\pi} U_d \cos(\frac{\Phi}{2}) \cdot \Omega_c \cdot C \cdot R}{\Omega_c^4 L^2 C^2 - 2\Omega_c^2 LC + 1 + \Omega_c^2 R^2 C^2}$$

$$U_{C_s} = \frac{\frac{4}{\pi} U_d \cos(\frac{\Phi}{2}) \cdot (1 - \Omega_c^2 \cdot L \cdot C)}{\Omega_c^4 L^2 C^2 - 2\Omega_c^2 LC + 1 + \Omega_c^2 R^2 C^2}$$

$$I_{0_c} = \frac{\frac{4}{\pi} U_d \cos(\frac{\Phi}{2}) \cdot \Omega_c \cdot C \cdot R \cdot (1 - \Omega_c^2 \cdot L \cdot C)}{\Omega_c^4 L^2 C^2 - 2\Omega_c^2 LC + 1 + \Omega_c^2 R^2 C^2}$$

$$I_{0_s} = \frac{\frac{4}{\pi} U_d \cos(\frac{\Phi}{2}) \cdot \Omega_c^2 \cdot C^2 \cdot R}{\Omega_c^4 L^2 C^2 - 2\Omega_c^2 LC + 1 + \Omega_c^2 R^2 C^2} \tag{11}$$

where $(U_{C_c}, U_{C_s}, I_{0_c}, I_{0_s}, \Omega_c, \Phi)$ are the values of the variables $(u_{C_c}, u_{C_s}, i_{0_c}, i_{0_s}, \omega_c, \phi)$ in the operating point.

The linearized model is found by perturbing the large-signal system given by (7)-(10) around the operating point. The perturbed variables are the inputs, the state variables, and the output. Each will have the form:

$$m(t) = M + \hat{m}(t), \tag{12}$$

where M is at the operating point, and $\hat{m}(t)$ is a small amplitude perturbation. Hence, these perturbed variables are replaced in (7)-(10) and then, by finding the Taylor expansion and considering only partial

derivatives, we obtain the linearized small-signal model:

$$\frac{d\hat{u}_{Cc}}{dt} = -\Omega_c \cdot \hat{u}_{Cs} + \frac{1}{C} \cdot \hat{i}_{0c} - U_{Cs} \cdot \hat{\omega}_c$$

$$\frac{d\hat{u}_{Cs}}{dt} = \Omega_c \cdot \hat{u}_{Cc} + \frac{1}{C} \cdot \hat{i}_{0s} + U_{Cc} \cdot \hat{\omega}_c$$

$$\frac{d\hat{i}_{0c}}{dt} = -\frac{1}{L} \cdot \hat{u}_{Cc} - \frac{R}{L} \cdot \hat{i}_{0c} - \Omega_c \cdot \hat{i}_{0s} - I_{0S} \cdot \hat{\omega}_c \quad (13)$$

$$\frac{d\hat{i}_{0s}}{dt} = -\frac{1}{L} \cdot \hat{u}_{Cs} + \Omega_c \cdot \hat{i}_{0c} - \frac{R}{L} \cdot \hat{i}_{0s} + I_{0C} \cdot \hat{\omega}_s + $$

$$+ E_{ui} \cdot \hat{u}_d - E_{\phi i} \cdot \hat{\phi}$$

$$\hat{p}_0 = R \cdot I_{0C} \cdot \hat{i}_{0c} + R \cdot I_{0S} \cdot \hat{i}_{0s}$$

B. Power Regulation Loop Small-Signal Model

Varying the duty cycle of the tank voltage regulates the output power. Fig. 4 shows the close loop for the power regulation, from which (after perturbing and linearizing), the following relationship for control angle $\hat{\phi}$ is obtained:

$$\hat{\phi} = K_\phi \cdot K_p \cdot \frac{Z_\phi}{R_2} \cdot \frac{e^{-sT_i}}{(s+a_p)R_1C_1} \cdot \tilde{p}_o =$$

$$= K_\phi \cdot K_p \cdot H_\phi \cdot \frac{e^{-sT_i}}{(s+a_p)R_1C_1} \cdot \tilde{p}_o \quad (14)$$

where K_ϕ is gain of the PWM, K_p is the total gain of the power sensor, H_ϕ is the compensator's transfer function, $\tilde{p}_o$ is the perturbed output power, and T_i takes into account the driver's propagation delay.

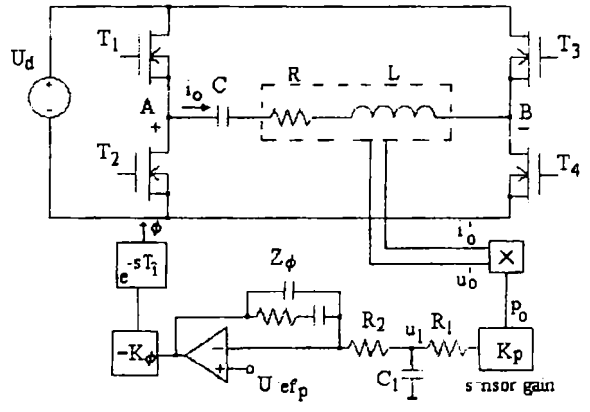

Fig.4. Power loop schematic

C. Frequency Loop Small-Signal Model

The frequency control circuit is composed of a charge measurement circuit, a compensator and a voltage-controlled oscillator (VCO), as show in Fig. 5. This circuit regulates the tank current charge during the ZVS transition to guarantee that ZVS is always achieved.

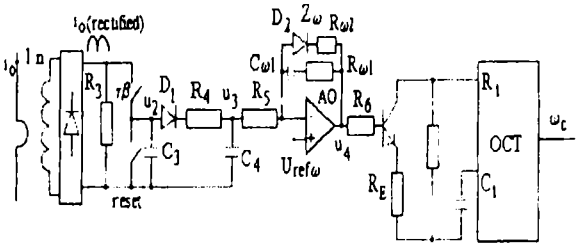

Fig.5. Frequency loop schematic

Small-signal model for frequency loop [1] is:

$$\hat{\omega}_c(s) = H_\omega(s) \cdot H_e(s) \cdot A \cdot (H_{i_{0C}\omega} \hat{i}_{0c}(z) + $$

$$+ H_{i_{0S}\omega} \hat{i}_{0s}(z) + E_{\omega\omega} \cdot \hat{\omega}_c(z) - E_{\phi\omega} \cdot \hat{\phi}(z)) \quad (15)$$

where A, $H_{i_{0C}\omega}$, $H_{i_{0S}\omega}$, $E_{\omega\omega}$ and $E_{\phi\omega}$ are coefficients that depend on the operating points [1]:

$$A = \begin{cases} 1, \text{if } u_2 > 0 \\ -1, \text{if } u_2 < 0 \end{cases} \quad (16)$$

$$H_{i_{0C}\omega} = KK \cdot \frac{I_{0s} \cdot e^{-a\frac{B}{\Omega_c}}}{(I_{0s}^2 + I_{0c}^2)} \cdot (-\frac{a}{\Omega_c} \cdot H_1 - H_2) +$$

$$+ KK \cdot e^{-a\frac{B}{\Omega_c}} \cdot (-\Omega_c \cdot \sin B + a \cdot \cos B) \quad (17)$$

$$H_{i_{0S}\omega} = KK \cdot \frac{I_{0c} \cdot e^{-a\frac{B}{\Omega_c}}}{(I_{0s}^2 + I_{0c}^2)} \cdot (\frac{a}{\Omega_c} \cdot H_1 + H_2) -$$

$$- KK \cdot (e^{-a\frac{B}{\Omega_c}} \cdot (a \cdot \sin B + \Omega_c \cdot \cos B) + \Omega_c) \quad (18)$$

$$E_{\omega\omega} = KK \cdot \left[I_{0s} - e^{-a\frac{B}{\Omega_C}} \cdot H_1 \cdot (\frac{aB}{\Omega_c^2} - \frac{2\Omega_c}{a^2 + \Omega_c^2}) \right] -$$

$$- KK \cdot e^{-a\frac{B}{\Omega_C}} \cdot (I_{0c} \cdot \sin B + I_{0s} \cdot \cos B) -$$

$$- KK \cdot \left[\frac{2\Omega_c}{a^2 + \Omega_c^2} \cdot (I_{0s} \cdot \Omega_c - I_{0c} \cdot a) \right] \quad (19)$$

$$E_{\phi\omega} = e^{-a\frac{B}{\Omega_c}} \cdot KK \cdot \left[\frac{a}{2 \cdot \Omega_c} \cdot H_1 + \frac{1}{2} \cdot H_2 \right] \quad (20)$$

with notation:

$$H_1 = (I_{0s} \cdot a + I_{0c} \cdot \Omega_c) \cdot \sin B + (I_{0s} \cdot \Omega_c - I_{0c} \cdot a) \cdot \cos B$$

$$H_2 = (-I_{0s} \cdot a + I_{0c} \cdot \Omega_c) \cdot \cos B + (I_{0s} \cdot \Omega_c - I_{0c} \cdot a) \cdot \sin B$$

$$KK = \frac{1}{n \cdot C_3 \cdot (a^2 + \Omega_c^2)} \quad ; \quad B = \beta\pi \qquad (21)$$

D Complete Small-Signal Model

The complete small-signal model implemented in PSPICE is shown in Fig. 6.

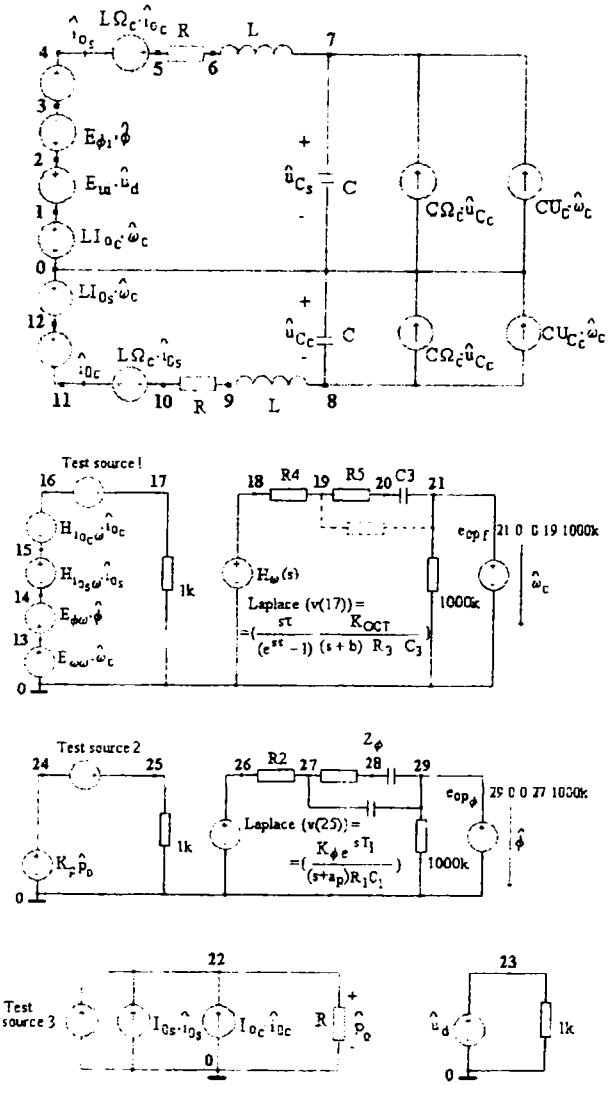

Fig.6.The complete small-signal model of series-resonant inverter

III. SIMULATION RESULTS

We have simulated the complete small-signal model in PSPICE. Our circuit's element values are:

R=16Ω ; L=12,4μH; C=12,76nF; N=6; Q=2,2; U_d=200V; P_{max}=2.5KW.

The parameters of the small-signal model for three values of the control angle $\hat{\phi}$ (three operating points) are listed in Table 1.

Table 1

Parameter	a) $\phi = 9^\circ$	b) $\phi = 45^\circ$	c) $\phi = 100^\circ$
f_c	442 kHz	450 kHz	468 kHz
Ω_c	2777167,9 s^{-1}	2827433,4 s^{-1}	2940530,7 s^{-1}
I_{OC}	-5,3567 A	-5,5739 A	-4,6062 A
I_{OS}	13,7848 A	12,1461 A	7,5119 A
U_{Cc}	-388,9993 V	-336,6619 V	-200,2034 V
U_{Cs}	-151,1632 V	-154, 4959 V	-122,7616 V
$L\Omega_C$	34,4368 Ω	35,0601 Ω	36,4626 Ω
L I_{OC}	-0,06642 mVs	-0,0691 mVs	-0,05711 mVs
L I_{OS}	0,1709 mVs	0,1506 mVs	0,0931 mVsv
$C\Omega_C$	0,035436 Ω^{-1}	0,036078 Ω^{-1}	0,037523 Ω^{-1}
C U_{Cc}	-4,963 μAs	-4,295 μAs	-2,554 μAs
C U_{Cs}	-1,928 μAs	-1,971 μAs	-1,566 μAs
$E_{\phi\omega}$	9,9897 $Vrad^{-1}$	48.724 $Vrad^{-1}$	97,5354 $Vrad^{-1}$
$E_{\omega\omega}$	-0,0138	-0,00154	0,0078
$H_{IOS\,\omega}$	-3,266e^3 Ω	-3,749e^3 Ω	-1,972e^3 Ω
$H_{IOC\,\omega}$	-19,773 e^3 Ω	-21,892 e^3 Ω	-24,366 e^3 Ω
$E_{\phi\omega}$	83,162 $e^3 Vrad^{-1}$	60,28$e^3 Vrad^{-1}$	22,854 $e^3 Vrad^{-1}$
$E_{\omega\omega}$	-0,01383 Vs	-0,00154 Vs	-0,00782 Vs

Simulation results are presented in Fig. 7 ÷ Fig. 9. From curves shows it can be seen that the frequency loop and power loop are stable. However our gains are relative low as well as the crossover frequencies. Modifications to the compensatory circuits can be made to increase the gain and crossover frequency. They can't be increased too much because of the possible saturation of AO from the compensator circuit of the frequency control circuit in case of negative error.

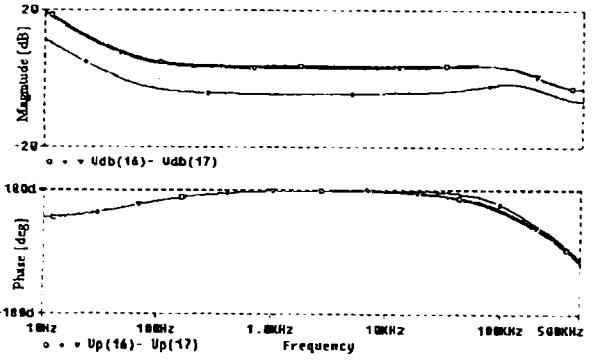

Fig.7. Frequency control loop gain for three operating points:

□ - $\phi = 9^\circ$; Δ - $\phi = 45^\circ$; ◊ - $\phi = 100^\circ$ (positive error)

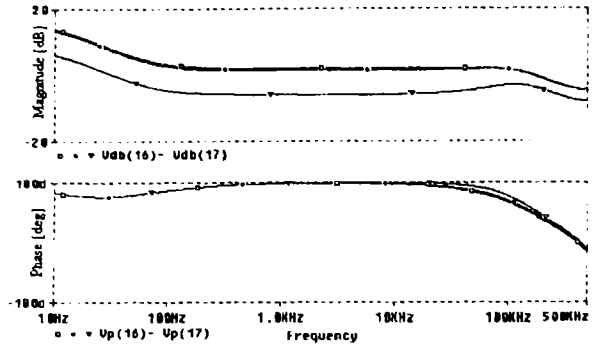

Fig 8 Frequency control loop gain for three operating points:

□ - $\phi = 9^\circ$, Δ - $\phi = 45^\circ$, ◊ - $\phi = 100^\circ$ (negative error)

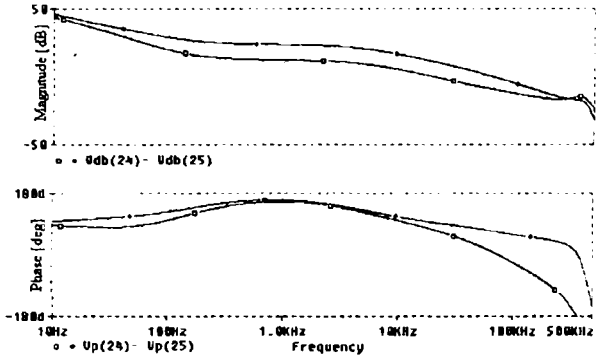

Fig.9. Power regulation loop gain for two operating points:

□ - $\phi = 9^\circ$; ◊ - $\phi = 45^\circ$

Because of the heating of the working piece the parameters of coil plus work-piece modify it's important to see wich are the influences of these modifications on the small-signal model of resonant inverter. The parameters of small-signal model for three different values of resistance R are presented in Table 2. The parameters of small-signal model for three different values of inductance L are presented in Table 3. The calculation was made for an control angle $\phi = 9^\circ$ and are presented only parameters wich suffer modifications of the values presented in Table 1, column a).

Table 2

Pa.a-meter	a) R=1 Ω	b) R= Ω	c) R= Ω
I_{OC}	-6,7263 A	-5,3567 A	-4,8174 A
I_{OS}	15,1468 A	13,7848 A	13,1719 A
U_{Cc}	-427,4501 V	-388,9993 V	-371,6852 V
U_{Cs}	-189,8142 V	-151,1632 V	-135,9395 V
L I_{OC}	-0,08340 mVs	-0,0664 mVs	-0,05597 mVs
L I_{OS}	0,1878 mVs	0,1709 mVs	0,1633 mVs
C U_{Cc}	-5,4537 μAs	-4,963 μAs	-4,7427 μAs
C U_{Cs}	-2,422 μAs	-1,928 μAs	-1,7346 μAs
$H_{IOS\omega}$	-3,9219e Ω	-3,266e Ω	-2,9878 e^3 Ω
$H_{IOC\omega}$	-19,724 e^3 Ω	-19,773 e^3 Ω	-19,742 e^3 Ω
$E_{\phi\omega}$	0 , 3 -1	, e^3Vrad^{-1}	79,491e^3 Vrad^{-1}
$E_{\omega\omega}$	-0,0198 Vs	-0,01383 Vs	-0,01182 Vs
τ	1,13e^{-6} s	1,11e^{-6} s	1,07e^{-6} s

Table 3

Para-meter	a) L=11.4uH	b) L=12.4uH	c) L=13.4uH
Ω_c	2890265 s^{-1}	2777167,9 s^{-1}	2627351,6 s^{-1}
I_{OC}	-5,1063 A	-5,5739 A	-4,7922 A
I_{OS}	14,0042 A	13,7848 A	14,2564 A
U_{Cc}	-379,7363 V	-388,9993 V	-425,22854 V
U_{Cs}	-1 8,456	-151,16	-1 3
$L\Omega_C$	32,9490Ω	34,4368 Ω	38,7295 Ω
L I_{OC}	-0,0582 mVs	-0,06642 mVs	-0,06421 mVs
L I_{OS}	0,1596 mVs	0,1709 mVs	0,1910 mVsv
$C\Omega_C$	0,036879Ω^{-1}	0,035436 Ω^{-1}	0,033525 Ω^{-1}
C U_{Cc}	-4,845 μAs	-4,963 μAs	-5,426 μAs
C U_{Cs}	-1,767 μAs	-1,928 μAs	-1,823 μAs
$H_{IOS\omega}$	-2,8719e^3 Ω	-3,266e^3 Ω	-2,7573e^3 Ω
$H_{IOC\omega}$	-18,601e^3 Ω	-19,77 e^3 Ω	-21,331 e^3 Ω
$E_{\phi\omega}$	77,16e^3 Vrad^{-1}	83,16e^3 Vrad^{-1}	79,491e^3Vrad^{-1}
$E_{\omega\omega}$	-0,0115 Vs	-0,01383 Vs	-0,0118 Vs

The simulation results are presented in Fig. 10-11 and show that the load rezistance growth makes to decrease gain of frequency control loop, while the load inductance growth makes this curls income higher. That's why, the projection of the frequency control loop must be made for high heating temperature of work-piece temperature at wich the load resistance it's the highest, and the value of load inductance is the lowest.

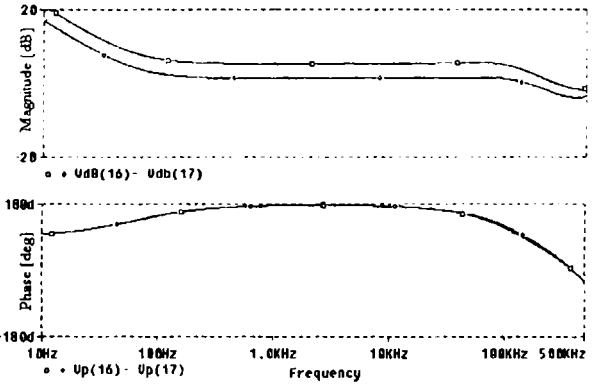

Fig.10. Frequency control loop gain for two values of R:

□ – R = 14 Ω; ◊ - R = 17 Ω

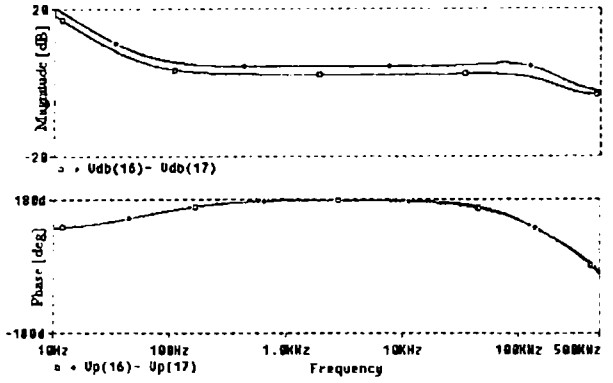

Fig.11. Frequency control loop gain for two values of L:
□ – L = 11,4μH; ◊ - L = 13,4μH

The transient response of resonant inverter at perturbations of input voltage is presented in Fig.12.

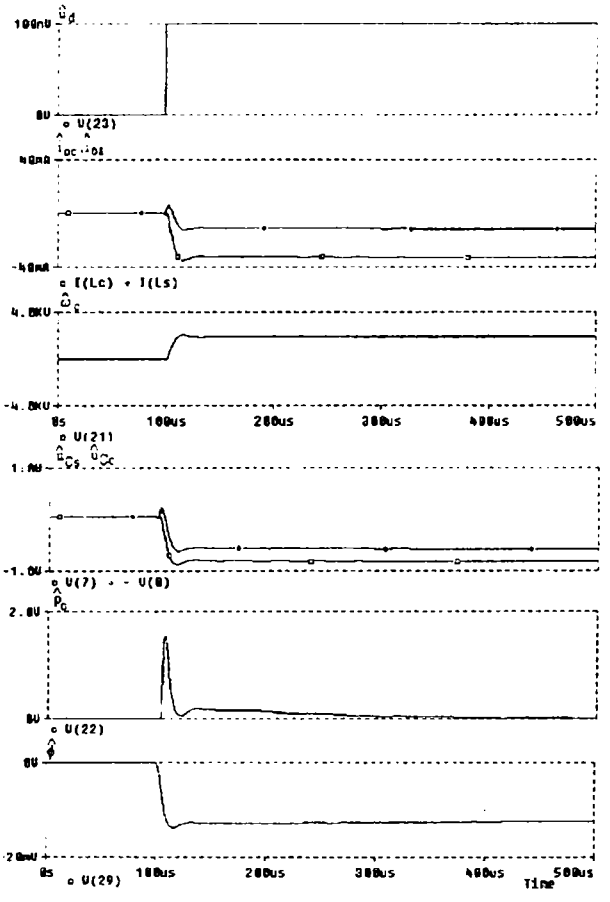

Fig.12. Transient response of the small-signal model

IV. CONCLUSIONS

In this paper, we present dynamic analysis of the phase-shift controlled series-resonant inverter for induction heating using harmonic approximation modeling. The small-signal model is used to study dynamic behavior of the resonant inverter. The results are obtained using PSPICE. Simulations verify the theoretical results.

REFERENCES

[1] L. Grajales, F. C. Lee, "Design of 10 kW, 500 kHz Phase-Shift Controlled Series-Resonant Inverter for Induction Heating", Proc. of Industry Applications Society, Toronto, Canada, 1993, pp. 843-849.

2. E. Yan , "Extended describing function technique applied to the modeling of resonant converters", *Proceedings of the Virginia Power Electronics Center Seminar*, Blacksburg, 1991 pp. 179-191.